RESEARCH ARTICLE

ADVANCED
PHYSICS
RESEARCH
Open Access

www.advphysicsres.com

Check for updates

Ultra-Inclined Nanocolumnar ZnO Films Sputtered Using a Novel Masking Configuration Providing Controlled and Restricted Oblique Angle Deposition for Enhanced Sensing Platforms

M. Pelayo Garcia, D. Gibson, K. L. McAughey, D.A. Hughes, and C. García Núñez*

Oblique angle deposition (OAD) of inclined thin films is mainly performed using electron beam evaporation due to its accurate point source control over the incoming evaporated flux angle α, leading to thin films with a nanocolumnar inclination angle β. However, the utilization of magnetron sputtering (MS) with an extended source for OAD is not extensively studied and reported. This work presents a thorough analysis of ZnO inclined thin films deposited by a novel restricted DC-reactive MS-OAD technique. OAD-inclined films are deposited at α ranged 60°-88°, where incoming flux is restricted using a patented masking configuration enabling tunable control of deposited nanocolumn angular range. The described technique provides accurate control over the resulting β (99.5% reproducibility), allowing demonstrated β_{max} of 47.3°, close to theoretical limits predicted for ZnO. The approach discussed here probes enhanced control of β comparable to that observed in evaporation, however using an extended source, resulting in high-quality reproducible nanocolumnar-inclined films. The mentioned improvements result from the exploration of operational parameters such as magnetron power, working pressure, and chamber temperature, as well as the design of the restricting configuration and substrate holders and their influence on the resulting inclined thin film crystallinity, and morphology.

M. Pelayo Garcia, D. Gibson, C. García Núñez
Institute of Thin Films
Sensors and Imaging
University of the West of Scotland
Scottish Universities Physics Alliance
Paisley PA1 2BE, UK
E-mail: carlos.garcianunez@glasgow.ac.uk
K. L. McAughey, D. Hughes
Novosound Ltd
Motherwell ML15UH, UK
C. García Núñez
Microelectronics Lab, James Watt School of Engineering
University of Glasgow
Glasgow G12 8QQ, UK

1. Introduction

Inclined nanostructured films have been widely used in such diverse fields, including sensing, energy storage, optical coatings, microfluidics or surface acoustic wave (SAW) devices (e.g., radio/TV transmitters, quantum acoustics, etc),[1–4] particularly for two main properties these materials possess. On the one hand, the extraordinarily high surface/area ratio enhances the performance and efficiency of sensing platforms.[5–8] On the other hand, the direct alteration of some intrinsic physical properties of the materials is possible when deposited under oblique angle conditions. Some applications include the creation of a magnetic anisotropy by means of altering the geometry of the film. This magnetic anisotropy is of particular interest for applications related to data storage devices.[9–12] In a particular example, researchers were able to increase the coercive field (H_C) of a Co_2FeAl thin film from 30 to 490 Oe when depositing the material under oblique angle deposition (OAD) conditions utilizing an incident angle (α) of 85°.[9] These results demonstrate the huge potential of OAD to enhance the physical properties of thin films, leading to a drastic improvement in the device performance. Another application generated by the structural anisotropy of inclined films was exploited in the field of optical coatings,[13,14] where different transparent conductive oxides (TCOs) deposited with the shape of inclined films – using OAD – exhibited unique birefringent properties.[15] Birefringence is a crucial property for optoelectronic devices, where manipulation of the optical properties of the materials is required. Some applications included the use of metal oxides such as Ta_2O_5, SiO_2, TiO_2, or Nb_2O_5 in Bragg's reflectors, waveguides, and other types of filtering.[16–18] Other examples would include the use of inclined materials for acoustics, specifically for ultrasonic sensing in liquid environments. It is well known that longitudinal mode (L-mode) waves dissipate energy in liquid media due to its coupling with liquid molecules,[19] however shear mode (S-mode) waves not. By inclining the structure of a piezoelectric film, the electromechanical coefficient for both modes can be tuned,

ADVANCED
SCIENCE NEWS

www.advancedsciencenews.com

ADVANCED
PHYSICS
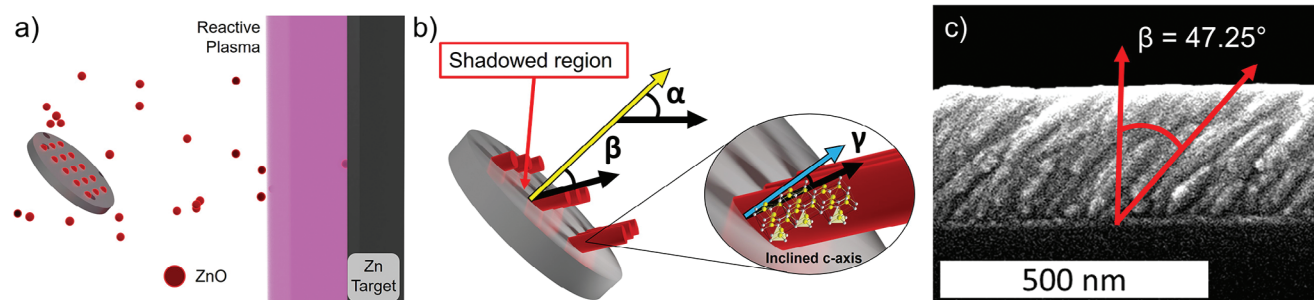**RESEARCH**
Open Access

www.advphysicsres.com

Figure 1. a) DC reactive magnetron sputtering deposition under OAD conditions 3D model. Metallic Zn target covered with a layer of ZnO oxide due to the reaction with an oxygen plasma O^{2-}. b) Representation of the characteristic angles belonging to a resulting film grown under an OAD process. The incident angle (α) is defined as the angle between the incident atomic flux and the normal vector of the substrate surface (marked with a yellow arrow). β represents the resulting column tilting angle. This angle is affected by the so-called shadowing effect (marked in red). The front structures that gas reaches first act as a mask for the substrate behind, making the layer grow in a tilted nanostructured manner. Inset: the zoom-in represents the third key angle of OAD films, the γ angle, which indicates the orientation of the crystalline c-axis. c) SEM image showing the record values of β achieved in this work on inclined nanostructured ZnO thin films.

suppressing the L-mode at a certain angle, therefore allowing the device to work more efficiently in liquids.[20–24] For example, it has been theoretically calculated that the electromechanical coefficient (k_{33}) is reduced to 0 when the structure inclination reaches an angle of 43°, consequently supressing completely any L-mode present in the excitation wave.[23] Achieving an inclined structure is not trivial for all materials, however its investigation is crucial for the development of the above technologies and new ones that are yet to come.

OAD is a method that consists of a well-known physical vapor deposition (PVD) under an inclined condition between the surface substrate and the incoming atomic flux, which results in a nanocolumnar inclined structure.[25] Typically, OAD processes are carried out using the PVD technique known as electron-beam assisted evaporation where a point source of atoms provides an accurate control of the shadowing mechanism where directionality is key.[26] Many studies, nevertheless, have tried in the past using an alternative PVD technique termed as magnetron sputtering (MS) given its better industrial scalability (i.e., faster, large area, and cheaper processes).[27,28] Using MS increases the complexity of the OAD process as the directionality is affected by the use of an extended distributed source of atoms and by the randomized directions of the incident particles when scattering processes occur due to the gas molecules colliding with each other in the discharge plasma. However, in terms of crystal growth, MS benefits from the ionic energy being high enough to promote crystal growth of the deposited material without any need for external heating, whereas evaporators require precise high substrate temperature, separate plasma ion assist, and pressure control to promote crystallinity, key for some applications involving piezoelectric materials (e.g., ultrasonic transducers, SAW devices, energy harvesting devices).[8] As stated, both e-beam evaporation and MS have been used to carry out the deposition of inclined thin films using OAD conditions, however, issues arise when discussing the uniformity, and thickness of the films, as well as the reproducibility of the process. In this regard, it remains a great challenge to generate successfully uniform inclined thin films and over large areas of devices which is hindering their deployment in the market, especially for the MS-OAD process.

In **Figure 1a** it could be observed the standard process occurring in a deposition of inclined films using DC reactive magnetron sputtering (DC-RMS). In that process, Zn atoms at the surface of the target are oxidized to ZnO, as the process is happening in the "poisoned" mode, and sputtered toward the surface of the substrate. As the material is being deposited, the molecules reaching the substrate surface are affected by the "shadowing effect" (Figure 1b). This effect directly depends on the relative angle, called α angle, between the incident flux angle (considered at the center of the target) and the substrate surface. The resulting film structure grows inclined with a certain angle, the β angle, that could be estimated by studying the morphology under scanning electron microscopy (SEM) as illustrated in Figure 1c. Additionally, a third angle must be taken into consideration when defining an OAD process, the γ angle, which represents the internal crystalline orientation of the c-axis, whose precise estimation is still unclear for some materials (*see* inset of Figure 1b). One proposed technique to characterize γ is the so-called χ-scan x-ray diffraction (XRD) analysis.[29]

The key concept to define an OAD process is the above-mentioned "shadowing effect", which is the principal governing mechanism for the structure to grow inclined (Figure 1c) when thermally activated diffusion processes are suppressed (i.e., no substrate/chamber heating applied during deposition).[26]

To overview the state-of-the-art OAD, **Table 1** shows a thorough comparison between β angles of some OAD materials ranging from metals to semiconductors reported in the literature using both electron-beam evaporation and MS. It could be observed how different inclined materials have been studied in the past for different applications, (*see* Remarks column in Table 1). Additionally, it shows how materials deposited by the use of electron-beam assisted evaporation allow the further increase of β as above-mentioned, in comparison to those grown by sputtering. Table 1 also proves how metals can be deposited under OAD conditions and achieve higher inclinations whereas binary or ternary compounds are limited due to the increase in their structural complexity.

Ultimately, Table 1 shows the highest values found in the literature to the best of our knowledge for OAD ZnO thin films by different deposition techniques. Above all, in this work, we report

Table 1. Comparative table with some OAD materials and their maximum achieved β angle.

Material	Technique	α angle	T (°C)[1]	β_{max} angle	Reference	Remarks
Ta_2O_5	Evaporation	85°	NIH	35°	[32, 33]	A theoretical model is presented accounting with surface trapping mechanism in good correlation with the experiments
SiO_2	Evaporation	80°	NIH	35°	[34]	Surface trapping mechanism is enhanced for metal-oxide species
TiO_2	Evaporation	60°	NIH	36°	[35]	Effective refractive index decreases when the β angle increases
ITO	Evaporation	85°	NIH	41°	[34, 36]	β values are found to lay in between metal and metal oxide tilting angles
ZnO	Sputtering	60°	150	34°	[37]	At an incline angle of 31° acoustic longitudinal mode is suppressed
	Sputtering	60°	NIH	30°	[38]	Inclined ZnO on Al foil generated mixed shear and longitudinal waves
	Sputtering	45°	200	40°	[39]	ZnO grown on self-standing diamond allows its further inclination
	Sputtering	35°	39	25°	[23]	ZnO grown on Si(100) using a SiO_2 buffer layer
	Sputtering	60°	120	34°	[40]	Inclined ZnO showed S-mode and Rayleigh waves were generated for SAW devices
	Sputtering	60°	NIH	47°	This work	Among all parameters, pressure, and flux restriction affect the most in MS-OAD processes. Record β values for ZnO.
TiN	Sputtering	65°	NIH	25°	[41]	Increase in electrical resistivity by tilting the structure. Structure also simulated with SIMTRA and MODENA MonteCarlo code (metallic sputtering mode).
AlN	Sputtering	80°	NIH	39°	[42]	Use of tilted AlN film as buffer layer for GaN LED. A blue shift of emission is observed
Ti	Evaporation	85°	NIH	56°	[32]	Metallic films are well described without considering surface trapping mechanisms
	Sputtering	89°	NIH	53°	[43]	Increased substrate temperature decrease β were observed. For low working pressure, the film grows more inclined. NASCAM MonteCarlo code is used to simulate the structure.
Au	Sputtering	85°	NIH	62°	[32]	Increased β angle when reducing Ar pressure in sputtering process. Demonstrated also with theoretical simulations.
Al	Evaporation	86°	NIH	54°	[44]	Change in the crystallite texture observed for films deposited at 77K
Ni	Evaporation	86°	-196	66°	[44]	Films deposited at 77K show an increase in β of 15° from its counterpart deposited at room temperature (300K)
TiZrN	Sputtering	85°	NIH	28°	[45]	Hardness of tilted samples shows lower values than flat-deposited films due to the increase of the film porosity
NiWO	Sputtering	87°	NIH	53°	[46]	Length, diameter, and β angle of the nanocolumns increase when increasing the Ni sputtering power

record values of β for both evaporators and sputtering deposition methods by optimizing the pressure and restricting the incoming flux of particles in a DC-RMS OAD process.

Understanding the correlation between the incident flux angle α and the resulting columnar tilting angle β has been thoroughly studied, ranging from basic geometrical models [26,44] to more advanced growth kinetics models based on Monte Carlo simulations.[45] Simulation and experimental research in the literature report that there is a critical angle in DC-MS OAD above which the material properties start to be affected by the inclined deposition.[46] However, due to the intricacy of the DC-RMS OAD of compound thin films (e.g., metal oxides or metal nitrides), no correlation has been established between α and β angle and also other input parameters (magnetron power, substrate temperature, and deposition pressure). The reactive component of the deposition brings a new level of complexity into the OAD mechanisms compared to standard metallic depositions. Additionally, the reproducibility of the obtained β angles is heavily affected by the randomized angular flux contributions naturally generated when using a large, distributed source of atoms. Im-

proving the directionality of the deposition could lead to an enhancement of the β angles, as directionality is crucial in OAD, hence its analysis is certainly relevant for the scope of this work.

In terms of magnetron power, it has been observed for some ternary materials (e.g., TiZrN, NiWO, see Table 1), the increase in sputtering power led to an increase in the aspect ratio and footprint of the resulting inclined nanocolumns.[42,43] Additionally, in terms of crystal quality, there exists a compromise between the crystallinity and the deposition rate. The higher the magnetron power, the faster the deposition but the less crystalline the resulting sample.[42] In regard to varying the substrate temperature, no definite conclusion has been achieved for all materials reported in the literature. Some studies indicate that the effect of elevated temperature on the resulting columnar tilting angle β is a material-dependent process.[41,47,48] Finally, in terms of deposition pressure, it has been observed in metals such as Ti or Au how reducing the working pressure in the chamber led to an increase in the resulting β angles (Table 1).[30,40] Investigating how the reduction in the working pressure could provide higher β columnar angles in more complex structures such as metal oxides is

**ADVANCED
SCIENCE NEWS**

www.advancedsciencenews.com

**ADVANCED
PHYSICS
RESEARCH**
Open Access

www.advphysicsres.com

particularly important to push even further the tilting of the resulting layers. However, that strongly depends on the deposition system capabilities, the best vacuum level one could obtain, and the temperature inside the chamber during the process.

For ZnO, only a few studies have been performed to explain the effect of the variation for some parameters (e.g., deposition parameters effect on ZnO:Ga material properties, and the use of a blind to block straight-line coming particles to reach the substrate).[49,50] Consequently, it is key for the analysis to understand MS-OAD inclined thin films for this specific material.

This work reports the advanced control of the inclined nanostructured ZnO thin films grown by DC-RMS under OAD conditions. This paper also shows the improvement of the β reproducibility between separate depositions and the significant increase of the columnar tilting angle β for nanostructured ZnO thin films beyond reported values (Table 1) and close to maximum theoretical calculations (*see* Section 3.2). Both are achieved by means of varying the deposition pressure (enhancing the ballistic conditions), by the use of the patented restricted mask configuration technology from Novosound Ltd,[51] which limits the angular components of the incident flux from the target, and optimizing the magnetron power and the substrate temperature of the deposition. It also reports the generated anisotropy of the inclination angles across the ZnO sample when depositing for longer times. Finally, for particular thin film devices where the thickness of the inclined piezoelectric film is required to be large (e.g., ultrasonic transducers),[28,52,53] growth kinetics of longer OAD processes have been studied.

2. Experimental Section

Prior to the OAD process, Si_{100} substrates (from University Wafers) were ultrasonicated in acetone for 5 min, and then in isopropyl alcohol (IPA) for another 5 min. Then, the substrates were dried under N_2 flow. Right after the cleaning, the samples were loaded into the growth chamber on customized substrate holders at different tilted angles (α). ZnO thin films were deposited by DC-RMS from a 100×300 mm^2 Zn target (99.99% purity) using O_2 and Ar as deposition gases (*see* Video S1, Supporting Information). The sputtering system comprises an industrial chamber with a drum that can allocate up to 56 samples of 20×20 mm^2 with a 70 mm distance between the sample and the target. The system has a dual independent DC magnetron system, allowing either co-deposition of multi-materials or a single material, controlled by constant power.

During the OAD process, the pressure variation was controlled by adjusting the total gas flow and the Ar/O_2 flow ratio using mass flow controllers (MFCs). The pressure was monitored throughout the deposition process using a cold-cathode ionization Penning gauge. For that study, the total Ar/O_2 flux was varied from 12 to 60 sccm (0.3 to 1.12 Pa), keeping the Ar/O_2 ratio at multiples of 5/10, to ensure a stoichiometric of ZnO films as demonstrated by energy-dispersive x-ray (EDX) analysis (*see* Figure S1, Supporting Information).

No intentional substrate heating was implemented, and the temperature stayed below 80 °C for the whole process. For the temperature study, a wire-bound radiant heater was utilized to bring the deposition chamber temperature (T_{ch}) up to 100 °C, the temperature was monitored by the use of a thermocouple sensor.

The temperature of the substrate is assumed to be equivalent to the temperature measured by the thermocouple. For every deposition before opening the shutters, the Zn target was sputtered with Ar for 15 min with a magnetron power of 400 W to ensure the elimination of any superficial oxide layer formed by the exposure of the target to the air. Additionally, the Zn target was sputtered with an oxygen-reactive plasma for 10 min at 300 W to allow the target to reach a stable oxidizing state. The deposition process is selected to occur in the "poisoned" mode of the reactive sputtering.

To investigate the correlation between α and β, a set of blocks (3D model of the blocks is available in Video S2, Supporting Information) was used to hold two samples at a designated angle (**Figure 2a**). For this study, we evaluated the columnar tilting angle for samples oriented at 0°, 60°, 70°, 80°, 84° and 88°. The minimum inclined angle selected was 60° as previous works suggested that α below this value does not produce films with significant β.[35] For the long deposition study, α angle of 80° was fixed constant and optimized sputtering parameters (i.e., 300 W magnetron power and 5/10 Ar/O_2) were utilized.

To deal with the reproducibility issue and the challenges found in MS-OAD associated with the use of a distributed source of atoms, this work proposes for the first time the use of the proprietary patented mask configuration technology by Novosound Ltd.[51] It consists of a restrictor box that ensures the complete elimination of angular components of the incoming flux (Figure 2b), allowing only the atoms coming in a line-of-sight from the target to reach the sample surface (Figure 2b, inset). The restrictor consists of a $100 \times 60 \times 40$ mm stainless steel box that encapsulates the angled block (sample holder) with a 60×20 mm rectangular slit that allows only the atoms coming in a straight line from the target to reach the sample surface (Figure 2c). Other slit configurations were tried prior to the optimal slit; however, no successful deposition was obtained, therefore is not shown in this manuscript. It included the use of a 60×5 mm and 60×50 mm slit. Every study, however, was carried out without the collimating technology unless specifically mentioned.

The morphology, composition, and structure of resulting inclined nanostructured ZnO films were characterized by SEM, EDX analysis (Cold field emission – Hitachi S4100), and XRD (Siemens D5000 Cu Kα, 40 kV/30 mA) with Bragg-Brentano configuration. The XRD scan comprised a $\theta/2\theta$ analysis from 2θ ranging from 20 to 70. The step size was set to 0.02 and the integration time was 1 s/step. The tilting angle of the resulting ZnO nanocolumns was estimated using the software ImageJ.[54] For calculation accuracy, 20 columnar angles were measured at 4 different sections of each sample and averaged to obtain the final value and standard deviation.

Finite element analysis (FEA) simulations were carried out using the Charged Particle Tracing module in COMSOL Multiphysics 6.1.[55] The simulation consisted of a 2D model of the deposition chamber used for the experiments in this work. From the 100×300 mm Zn target, 10 random particles were sputtered every 0.01s for 0.5s, with non-uniform velocities following a cosine distribution from the target surface. Collisions between released particles were allowed and modeled to simulate the actual deposition process where collisions can interfere with the directionality of the deposition. To define the collision
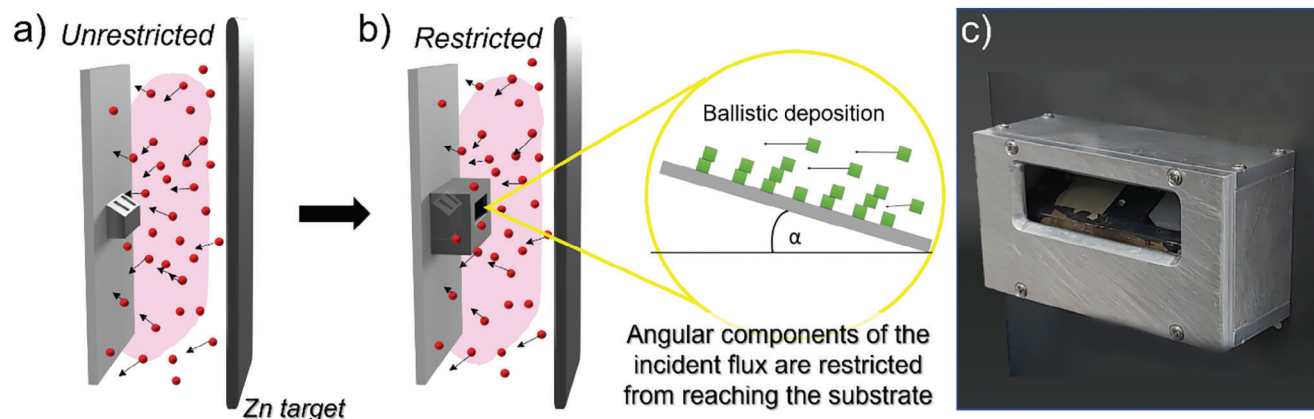
Figure 2. a) OAD schematic representing the randomness generated in an unrestricted deposition process and the angled block used to hold the samples at an angle α. b) OAD schematic representing the increase in directionality when restricting the incident flux with a mask, where only the vectors flowing in a straight line are allowed to reach the sample surface. c) Actual restrictor box used to mask the angular components of the incident gas flux; the α-angled block (sample holder) can be observed through the slit. Technology patented by Novosound Ltd.[51]

probability, 300K is used as the temperature of the chamber, 10^{20} m^{-3} is the background gas density, and 1.35×10^{-25} is used as the background mass for the sum of Ar and ZnO, and a collision frequency of 2 MHz is used as default (more details can be found in the Supplementary Material). A 20×20 mm^2 substrate was placed at 70 mm distance from the center of the target, and its surface was selected as a particle counter, allowing the quantification and the position of the particles reaching the surface of the substrate. For the restricted simulation a top and bottom wall was modeled and placed in between the target and the substrate, simulating the restrictor mask configuration technology described above. Any particle touching that wall was immediately removed during the simulation.

3. Results and Discussion

3.1. Magnetron Power Optimization

Figure 3a shows SEM images of inclined films deposited at different magnetron powers ranging from 50 to 400 W, keeping constant a pressure of 0.3 Pa (corresponding to an Ar/O$_2$ flux ratio of 5/10) and a substrate angle α of 60° for testing under OAD conditions. It is observed how the columnar structure is compromised when depositing at low (50 W) or high (400 W) magnetron power, whereas for intermediate power it remains a well-defined columnar structure. It is important to note how the deposition rate (r_g) increases when the magnetron power increases, as expected, ranging r_g from 0.06 to 0.8 µm h^{-1} from low to high power. To characterize the crystal quality of the deposited film for diverse power, XRD studies were performed. Figure 3b shows the resulting XRD patterns for different magnetron power values. It is observed the crystal is oriented primarily along the (002) crystallographic plane for all samples (wurtzite c-axis normal to the substrate surface), with the (100) orientation appearing with a relative intensity of ≈2% with respect to the dominant peak. Figure 3c shows the peak position 2θ as a function of the magnetron power. It is observed for all samples how there exists some intrinsic tensile residual stress from the deposition as the (002) peak appears shifted compared to the expected peak position for

that crystallographic plane, natural when depositing material under OAD conditions.[56] From Bragg's law (Equation 1):

$$n\lambda = 2d \sin\theta \tag{1}$$

where λ represents the wavelength of the used X-ray, d is the interplanar distance, and θ the peak position. It could be extracted that a decrease in the peak position θ would be a consequence of an increase in the interplanar distance d, in other words, an indication of tensile stress in the lattice, for the same wavelength. It is well known that the lower the magnetron power, the lower the resulting deposition rate. As seen in other works, an increase in the deposition rate would result in an increment in the structure stress.[57]

To accurately quantify the crystal quality, the crystal grain size was calculated by the use of the Scherrer equation.[58] Figure 3d demonstrates the largest crystal grain size among all the studied magnetron power values is achieved by depositing at 300 W which indicates a better crystallinity,[58] in agreement with the morphology extracted from the SEM analysis. From the figure, three different areas are observed. The first zone appearing at low magnetron power is called the ultra-thin film area. Here the film shows low crystallinity attributed to a lack of crystal material, in other words, the thickness of the material is not enough to contribute significantly to the XRD signal. The second zone would correspond to the optimal crystal quality, it is achieved at a deposition magnetron power of 300 W. This is the goal zone to obtain a good crystal, therefore enhancing the piezoelectric properties. Finally, the last zone, achieved at high magnetron powers is here called the high-defect density area, referring to the issues that bring to the resulting piezoelectric output. Above 300 W, the material seems to increase its polycrystallinity by the appearance of other crystal planes of the ZnO structure. That is observed in the appearance of new crystal planes (i.e. (100) and (101)), seen at 400 W in Figure 3b; and the reduction of the (002) peak intensity. Also, some Zn phase defects start to appear when depositing at 350 W as seen also in Figure 3b. The study concluded that 300 W was the optimum power for achieving a great crystal quality, as demonstrated by XRD analysis (Figure 3b,d), whilst
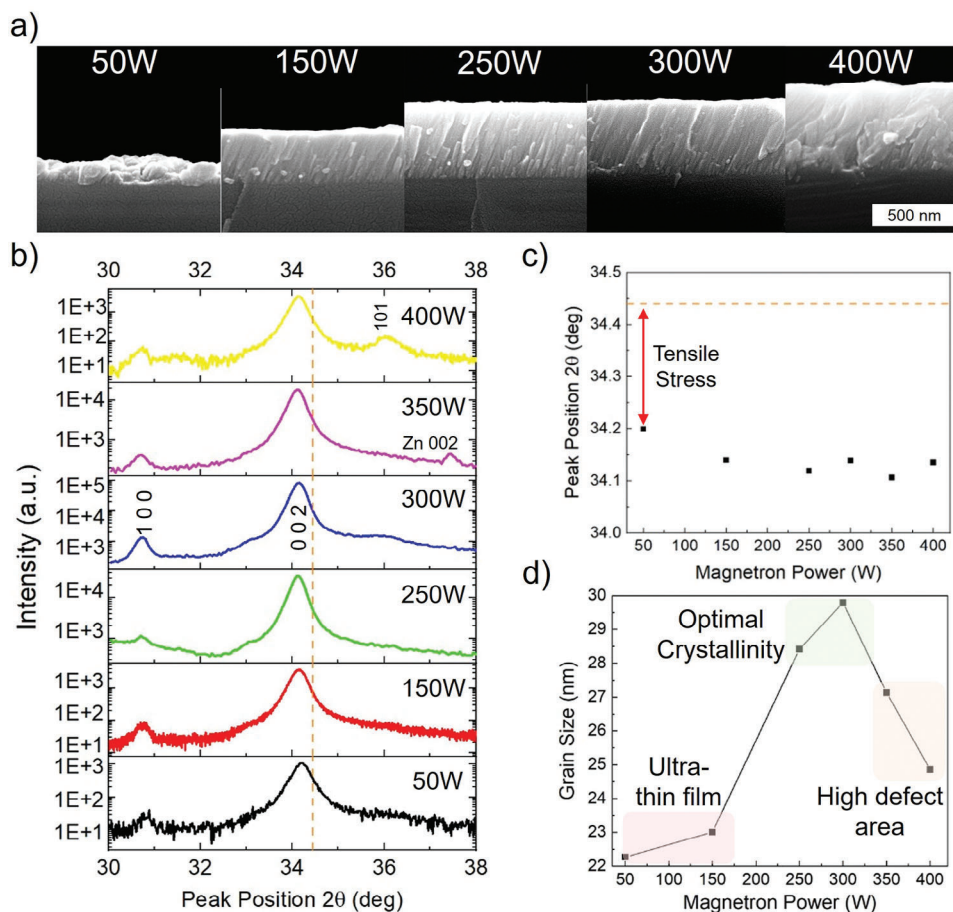
**ADVANCED
SCIENCE NEWS**

www.advancedsciencenews.com

**ADVANCED
PHYSICS
RESEARCH**
Open Access

www.advphysicsres.com

Figure 3. a) SEM images for ZnO films deposited at $\alpha = 60°$, 0.3 Pa total pressure, at different magnetron power values for optimization purposes. b) XRD pattern for samples deposited for the magnetron power calibration (400 to 50 W, from top to bottom). Marked with an orange dashed line is represented the bulk ZnO (002) crystallographic plane diffraction angle at $2\theta = 34.44°$ (extracted from crystallographic database card JCPDS 36–1451). c) Peak position 2θ as a function of the magnetron power calculated by fitting a Voigt function around the 002 diffraction peak (more details in Figure S2, Supporting Information). A negative shift in all deposited samples is observed compared to the bulk (002) expected ZnO peak (indicated with an orange dashed line), suggesting tensile stress is a consequence of the resulting deposition. d) Grain size calculated with the Scherrer equation as a function of magnetron power. Three subgroups are extracted from the results. The first group is labeled in the graph as the ultra-thin film area. The second subgroup is seen in the region where the optimal crystallinity is achieved at 300 W. Finally, observed for high deposition powers, the high density of defects area. For these reasons, 300 W is chosen as optimum keeping the balance between deposition rate (r_g) and crystal quality.

keeping a good compromise with the film thickness (Figure 3a). This optimized power is utilized then in all depositions, achieving $r_g \sim 0.6 \, \mu m \, h^{-1}$ (measured in samples mounted at $\alpha = 0°$).

3.2. Pressure Influence on ZnO Film Columnar Angle

SEM analysis indicates that reducing the total gas flux (and thus the pressure) leads to an increase in the resulting columnar tilting angle β for a chosen angle α of 80° (**Figure** 4a,b,c). SEM images demonstrate for the first time in ZnO OAD films, to the best of our knowledge, that just by decreasing the pressure from 1.11 to 0.3 Pa an increase from $\beta = 8 \pm 2°$ to $\beta = 23 \pm 2°$ is observed for the same deposition conditions. This effect has been previously observed only in metals such as Ti or Au thin films,[30,40] however not in more complex binary structures such as metal oxides. By reducing the working pressure, one could limit the interaction between the sputtered atoms and the gases inside the

chamber, leading to a more directional deposition. This interaction, in other words, probability of collision, is directly related, in a first-order approximation, to the mean free path (MFP) of the sputtered atoms, in our case ZnO (λ_{ZnO}), which is inversely proportional to the working pressure in the chamber during deposition (Equation 2),

$$\lambda_{ZnO} = \frac{k_B T_{ch}}{\sqrt{2} d^2 \pi P} \tag{2}$$

where k_B is the Boltzmann constant, T_{ch} is the deposition chamber temperature (K), P is the working pressure (Pa), and d is the diameter of the gas particles (m).

Figure 4d demonstrates the successful ballistic growth improvement in an OAD process, caused by fewer interatomic collisions when increasing the MFP (Figure 4e), which is in good agreement with results observed in metals.[30,40] From Figure 4d it is observed that the nanocolumn inclination angle β appears

**ADVANCED
SCIENCE NEWS**

www.advancedsciencenews.com

**ADVANCED
PHYSICS
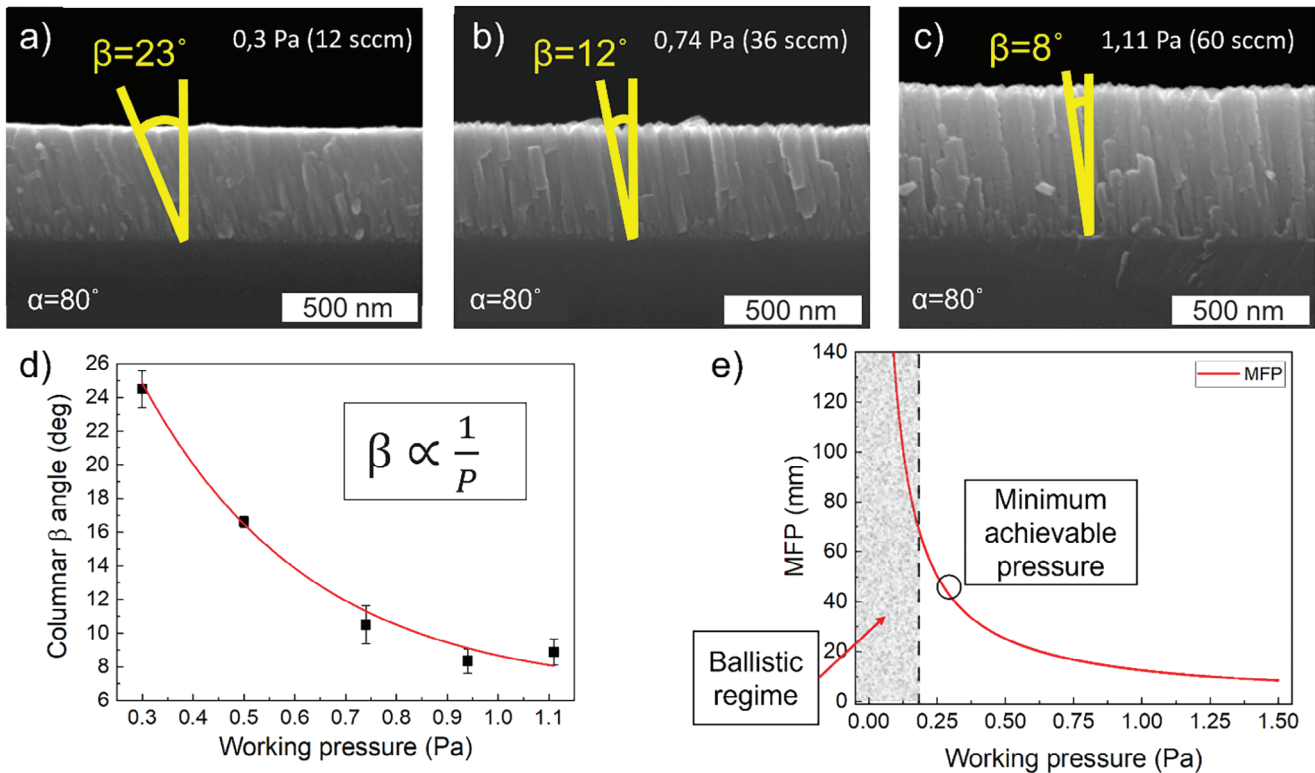RESEARCH**
Open Access

www.advphysicsres.com

Figure 4. a–c) SEM analysis for samples deposited at different working pressures; 0.3, 0.74, and 1.11 Pa, respectively. It is observed that lower working pressure leads to larger β angles. d) Resulting tilting angle β as a function of the total flux during deposition. There is an observable exponential decay trend of a decrease in β when increasing the working pressure. e) Mean-free path graph representation for ZnO as a function of the working pressure.

inversely proportional to the working pressure, indicating a higher effect on β would be expected if the deposition system could reach pressures below 0.3 Pa. In the graph represented in Figure 4e, it can be seen the modeled MFP as a function of the working pressure following Equation 2. Ideally, one would aim to increase the MFP over the target-to-sample distance, which would ensure no interatomic collision of the ZnO sputtered atoms on their path toward the substrate, in other words, ideal ballistic conditions that would maximize the tilting of the crystal structure (high directionality). In our specific study, the ZnO MFP (λ_{ZnO}) ranged from 11 to 42 mm, for 1.1 to 0.3 Pa, respectively. Given the target-to-sample distance is 70 mm, one could observe how reducing the pressure the ballistic conditions are optimized (Figure 4e, indicated with a black circle), however not yet achieving a complete ballistic regime.

For short MFPs, the atoms reaching the surface of the substrate have a wide distribution of incident angles, caused by scattering processes, leading to a decrease in the structure inclination. When the pressure is reduced, the particles reaching the sample suffer fewer collisions, therefore exhibiting smaller angular distribution, all in all resulting in high-tilted nanocolumnar films.

The optimum pressure achieved with the utilized deposition system is 0.3 Pa (corresponding to an MFP of 42 mm) and is used for the restricted sputtering and deposition time studies. To the best of our knowledge, this is the first report on ZnO thin films demonstrating the decrease of working pressure leading to enhanced tilted films (Figure 4d).

3.3. Restricted Sputtering Flux Effect on ZnO Film Columnar Angle

3.3.1. Control and Reproducibility In Restricted And Non-Restricted Conditions

SEM images were used to compare the morphology of inclined films deposited under non-restricted and restricted conditions (see Figure 2 in the Experimental Section) using different α angles. From **Figure 5a**, we can observe the evolution of both non-restricted and restricted ZnO thin films as a function of the incident flux angle α. For non-restricted films, it is observed how the columnar angle β increases as we increase α, specifically when changing from 60° to 70°. Also, it can be observed how the film thickness is reduced when increasing the incident flux angle α, that associated to the natural reduction of the total flux reaching the surface substrate. For restricted conditions, we observe a similar effect on the thickness, however for the columnar angles a different trend is observed. The effect of α in β is lower than observed in non-restricted conditions (this effect will be discussed further in relation to Figure 5c).

All in all, comparing non-restricted with restricted conditions, it can be concluded that the use of a restrictor box increases β values for the same set of deposition parameters, however the percentage of increase changes when changing α, as will be discussed later on with Figure 4d. Moreover, it is also observed that the restrictor box has a drastic effect on the deposition rate mainly due to the reduction of the effective elements arriving at the
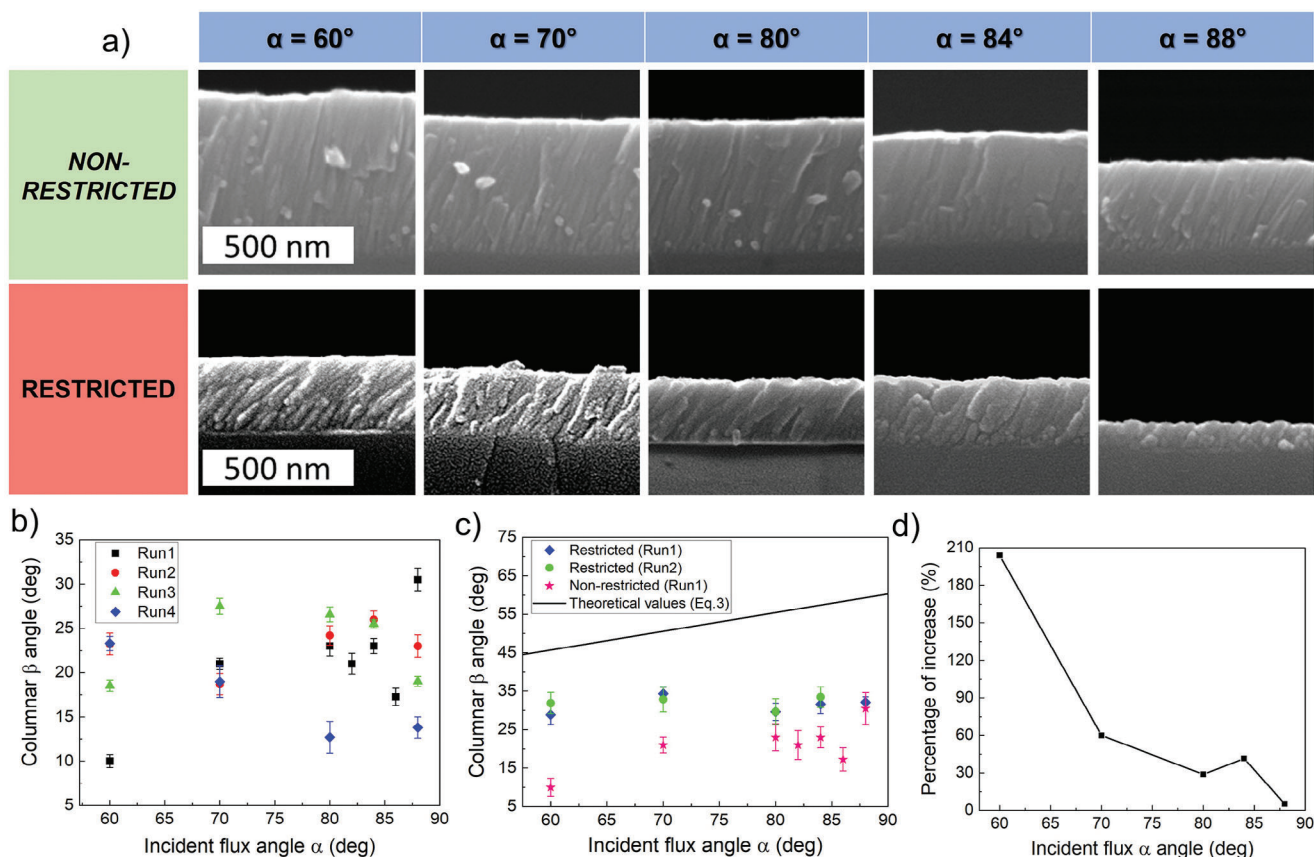
**ADVANCED
SCIENCE NEWS**

www.advancedsciencenews.com

**ADVANCED
PHYSICS
RESEARCH**
Open Access

www.advphysicsres.com

Figure 5. a) SEM images for different OAD nanostructured ZnO films deposited at different incident flux α angles. The top row corresponds to samples deposited without restricting the incident flux whereas the bottom row corresponds to samples grown under a restricted flux of atoms. b) Resulting tilting angle β as a function of the incident flux angle α for different non-restricted depositions. It is clearly observed how the reproducibility between separate runs is an issue in obtaining a consistent deposition method. Each data point corresponds to 20 analyzed nanocolumns inclination angles in three different locations of the sample separated 5 mm, which shows great uniformity across the sample. c) Resulting tilting angle β as a function of the incident flux angle α for non-restricted, restricted (restrictor box[51]) and theoretical calculations using the cosine rule.[59] d) Percentage of increase in β angles versus incident flux α angle when utilizing a restricted flux of atoms in comparison with the non-restricted growth.

surface of the substrate, resulting from the collimation and masking of the sputtered atoms.

Figure 5b shows a dispersion of points corresponding to different runs carried out at various α angles ranging from 60° to 88° for non-restricted conditions. In that figure, one could conclude that the level of reproducibility is low, mainly due to the large size of the target used in OAD, which is one of the main issues when running OAD in sputtering.[26] The restrictor box, in counterpart, has also been observed to have an effect on the reproducibility of the film growth. In order to understand better the role of the restrictor box on the reproducibility of the deposition, we have quantified the reproducibility (R) of the runs under both experimental conditions (i.e., with and without restriction). The difference in the beta angles obtained between runs is quantified as $\beta = \bar{\beta} \pm \delta\beta$, where $\bar{\beta}$ is the mean of the β and $\delta\beta$ is the standard error calculated as $\delta\beta = \sigma/\sqrt{n}$, where σ is the standard deviation and n the number of separate runs. Here, the $\delta\beta$ is called R, reproducibility. Figure 5c shows the resulting β angle for two separate runs under restricted conditions. Calculating the new reproducibility parameter R from Figure 5b,c, it could be observed how the angle distribution between separate runs has been reduced for the different sets of α angles. Averag-

ing the non-restricted R (Figure 5b) along all sets of angles, an R of 4.8 is obtained, whereas it is reduced to 1.5 when restricting the incoming flux (Figure 5c). Consequently, confirming the improvement of the β angle control by using the patented restricting technology [51] that masks the angular components of the incident atomic flux, therefore improving the directionality of the deposition. More details on the difference between restricted and non-restricted incident atomic flux limitation has been modeled using FEA and will be discussed next with **Figure 6**.

The relationship between α and β in inclined films deposited under OAD conditions have been theoretically modelled through a number of different expressions, though they often fail when estimating the β angle for PVD processes. The tangent rule, for example, is demonstrated to provide accurate estimations of β only when α is kept below 60°, failing for higher incidence angles.[44] For the sake of comparison in Figure 5c it can be observed the β values compared with the theoretical model explained by Tait et al.[59] This model, the so-called cosine rule (Equation 3), assumes a fixed relation between β and α. This relation does not take into account any material property or deposition parameters, it is purely geometric. Also, it predicts the relation considering ideal ballistic conditions.
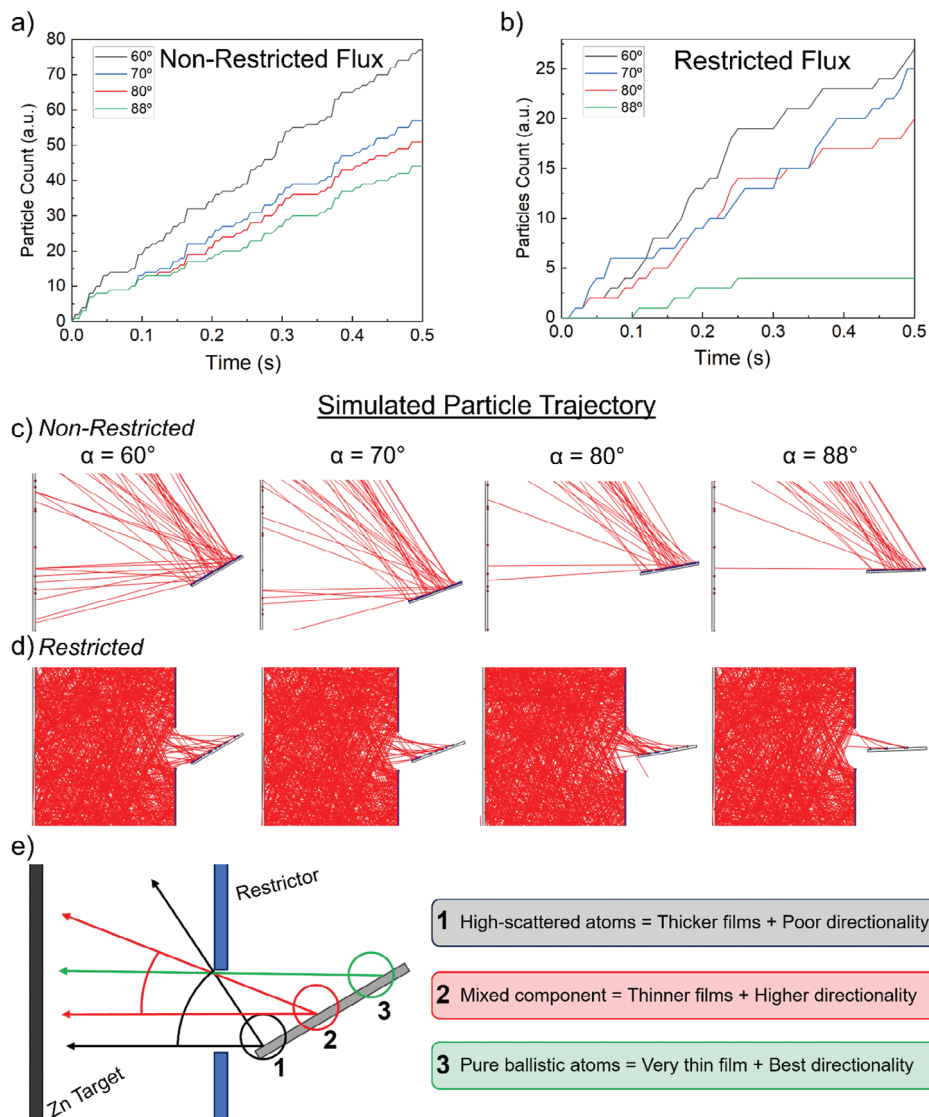
ADVANCED
SCIENCE NEWS

www.advancedsciencenews.com

ADVANCED
PHYSICS
RESEARCH
Open Access

www.advphysicsres.com

Figure 6. a) Particle count on a 25 × 25 mm² substrate placed 70 mm from a 100 × 300 mm² Zn target as a function of time for incident flux angles of 60°, 70°, 80° and 88° with non-restricted conditions. It can be seen how for higher α the particles reaching the substrate surface are reduced by the geometrical limitation. b) Particle count on a 25 × 25 mm² substrate placed 70 mm from a 100 × 300 mm² Zn target as a function of time for incident flux angles of 60°, 70°, 80° and 88° with restricted conditions. It is observed how the total number of particles reaching the surface of the substrate is reduced compared to non-restricted conditions, however it improves drastically the directionality of the deposition. c) Finite element analysis simulated particle trajectories in a deposition process under non-restricted conditions for the studied incident flux angles α of 60°, 70°, 80°, and 88°. It is observed the poor directionality of the process that results in a low inclination OAD film. The trajectories not reaching the surface of the substrate are eliminated from the simulation, therefore do not appear in the result. d) Finite element analysis simulated particle trajectories in a deposition process under restricted conditions for the studied incident flux angles α of 60°, 70°, 80°, and 88°. The restricting technology [51] limits the high angular components of the incident flux to reach the surface of the substrate, increasing the directionality of the deposition. The complete simulation sequence for all the studied angles and both restricted and non-restricted conditions is available in Videos S3–S6 (Supporting Information). The trajectories reaching either the restrictor wall or the surface of the substrate remains in the screen. e) Schematic of the three areas with different angular exposure for restricted OAD processes. Area 1, also called "front", has the biggest angular variation in the particles reaching the substrate due to the closeness to the restrictor. It also has the highest exposure to the sputtered atoms (i.e., thicker area in the film). Area 2 comprises a mixture of both the "front" and the "back", the angular distribution of the atoms is lowered, and the atomic contribution is reduced. Area 3, also called "back", corresponds to the area where only pure ballistic atoms can reach, therefore the directionality of the deposition is maximized, obtaining the best OAD conditions.

$$\beta = \alpha - \sin^{-1}\left(\frac{1-\cos(\alpha)}{2}\right) \tag{3}$$

To give an exact relationship between the critical angles for all materials is not trivial, therefore one must consider each spe-

cific material and deposition configuration when developing a theoretical model.[45] From Figure 5c it can be observed how the values of β obtained under non-restricted conditions follow the upward trend observed in the cosine rule. That suggests that α is affecting the resulting columnar angle β, following the slope

ADVANCED
SCIENCE NEWS

www.advancedsciencenews.com

ADVANCED
PHYSICS
RESEARCH
Open Access

www.advphysicsres.com

observed from Equation 3. In counterpart, for restricted conditions, a different effect is observed. The columnar angle β no longer depends on the incident angle α for the studied angles. However, there is an overall increase in β when compared to the non-restricted conditions, for the same deposition parameters. This demonstrates that the use of the restricting technology[51] is efficient in pushing the limits in obtaining higher columnar angles β. Figure 5d describes the drastic effect of restricted OAD on β, compared to non-restricted conditions. The restricting effect on β is observed to be maximized when using low incident flux angles ($\alpha \approx 60°$), reaching an improvement of 20° (200% increase) with respect to the non-restricted sample. Whereas for higher angles ($\alpha \geq 80°$) the increment lies between 2–6° (10-30%) increase (Figure 5d). This result could be explained by the intrinsic improvement of the shadowing effect when at low angles the incident flux is maximized. Using a high-angle substrate holder increases the restricted area due to the intrinsic geometry of the restrictor box (Figure 2d), therefore limiting the density of atoms reaching the surface of the sample. The increase in the collimation when increasing the incident angle α leads to fewer atoms contributing to the shadowing effect. In other words, there exists a compromise between the chosen α and the amount of incident flux reaching the sample surface. To further understand this effect, modeling the particle trajectories in a deposition process using FEA simulations was carried out.

3.3.2. Study of The Anisotropy In Restricted and Non-Restricted Conditions

Figure 6a,b show the simulated number of particles reaching the substrate of the sample for the studied angles ($\alpha = 60°$, 70°, 80°, and 88°) as a function of time, for both restricted and non-restricted deposition conditions, respectively. It is observed, as seen empirically (Figure 5a), that the number of particles reaching the substrate decreases as we increase the incident angle, as mentioned before, for both restricted and non-restricted depositions, therefore reducing the thickness of the film. Additionally, it is confirmed that restricting the flux limits the total number of particles reaching the substrate, therefore reducing even more the thickness of the resulting film (Figure 6b). From the simulated particle trajectory, we could observe how for non-restricted conditions the desired directionality of the deposition is compromised due to the larger size of the metallic target compared to the substrate (Figure 6c). Most particles reaching the substrate follow a perpendicular direction with some contributing to the directionality required for the shadowing effect to occur. In Figure 6d however, when the restrictor is blocking the undesired angular components of the flux, it can be observed how the particles reaching the substrate follow a more directional trajectory, therefore allowing the atoms to reach the substrate at the desired angle that contributes for a successful oblique angle deposition. Additionally, from the simulations under restricted conditions, it could be observed how there are different areas within the substrate where different incident angles reach. Figure 6e represents in a diagram the three areas we could divide the substrate when depositing under restricted OAD conditions. The first area is the one called here the "front" of the sample, and the closest to the target and to the restrictor aperture. Whereas most of the unde-

sired high angular components of the flux have been blocked by the restrictor, area 1 is exposed to a higher influence of diverse angles (highly scattered atoms) reaching the substrate. That results in a less directional deposition (i.e., smaller columnar inclination angles β), but a higher number of particles reaching the substrate (i.e., increased thickness). For the second area, that located in the middle of the sample, it can be observed how the angles of the particles reaching the substrate are reduced, therefore augmenting the directionality, but it is still open enough for diverse angular components of the flux to reach and deposit. Finally, the last area, called here the "back" of the sample, is the furthest part from the target. Only the atoms with a straight line-of-sight directionality coming from the target will reach and contribute to the growth. As the restriction is maximal in area 3, the atomic contribution is low therefore the thickness in that area would be the lowest in the sample. However, the directionality is at its best, as only ballistic particles will reach, therefore the best conditions for OAD (i.e., highest β angles).

To demonstrate what was observed in the simulation studies, cross-section SEM analysis was performed along different sections of a sample deposited under restricted conditions at $\alpha = 60°$, to ensure high atomic contribution, as discussed earlier. From **Figure 7a**, it is demonstrated the existence of anisotropy in the inclination angles and thickness across the sample, especially for lower α, as seen from the simulations (Figure 6e). Also, from Figure 7a, it is observed how the thickness across the sample, following the direction of the growth, varies, with the "back" of the sample being the thinnest, and the "front" the thickest. This anisotropy can even be spotted by the naked eye. In Figure 7b it can be observed the bare difference between films grown under non-restricted and restricted conditions. The difference in the optical diffractive patterns indicates there exists a variation in the film thickness along the sample, as predicted by FEA simulations (Figure 6e). To further understand this effect on the structural inclination of thin films, the β angles and thickness were extracted from the SEM images (Figure 7a). Figure 7c represents the evolution of the β angle and the thickness across a single sample deposited at $\alpha = 60°$ (to enhance the shadowing effect, consequently its inclination) from its "front" (shortest target-to-sample distance) to the "back". From the figure, it is observed how the thickness varies from 150 ± 6 nm to 697 ± 19 nm (which corresponds to ≈78% total change) when moving from the "back" of the sample to the "front", indicating the level of anisotropy of the deposition. In terms of β, it is observed a 69% increase in the inclination from the "front" to the "back", reaching the highest values at the furthest part of the sample, in other words, at the "back" of the sample.

Both morphological analysis and visual inspection, together with the simulations of the inclined films confirm the existence of a gradual increase in the inclination when moving from the "front" side (i.e., the first area the incident flux reaches in the sample) toward the "back" side of the restricted OAD sample. This particular effect is explained by the exacerbation of the self-shadowing effect from the front columns to the rest of the sample. When the flux is restricted, the atoms reaching the back of the samples are limited to those coming in a straight line and, therefore are subjected to a strong shadowing effect from the atoms deposited at the front. This effect is naturally achieved when depositing using an electron-beam deposition as its source of atoms
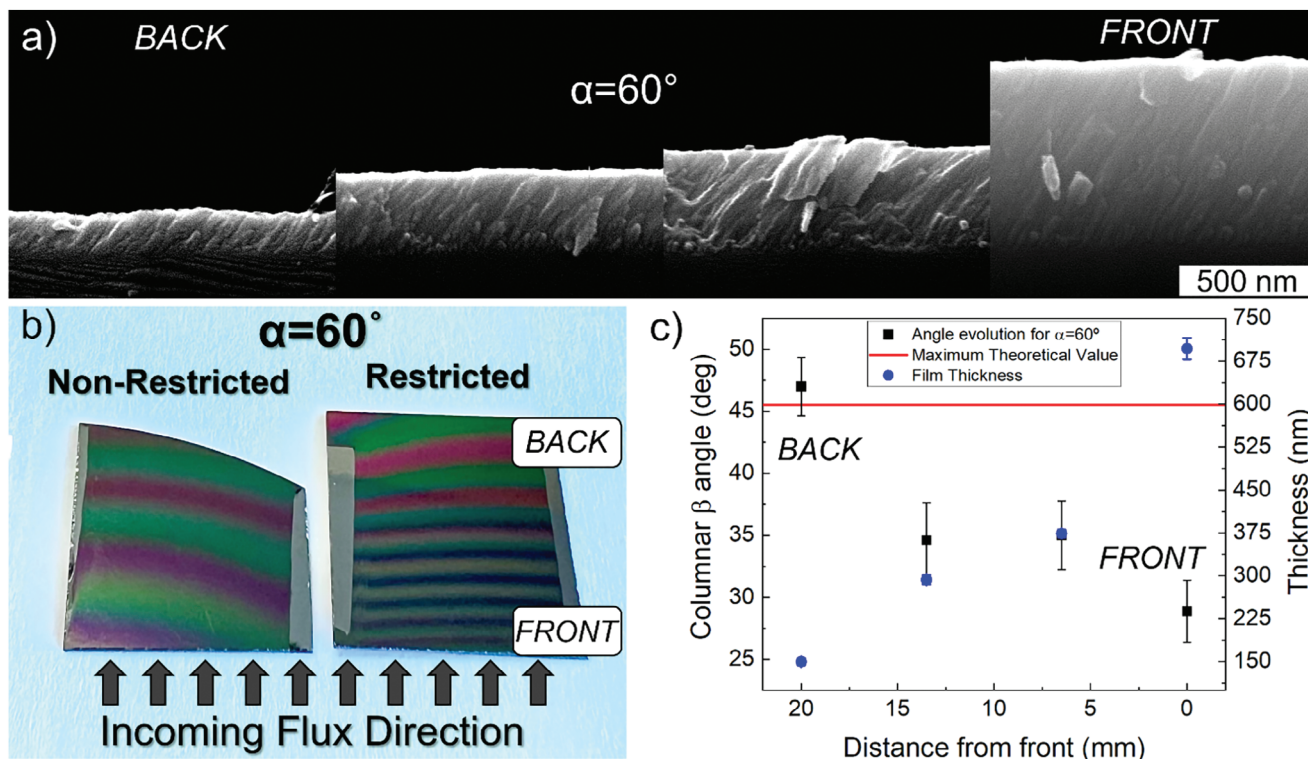
**ADVANCED
SCIENCE NEWS**

www.advancedsciencenews.com

**ADVANCED
PHYSICS
RESEARCH**
Open Access

www.advphysicsres.com

Figure 7. a) SEM analysis across a single sample deposited under OAD restricted conditions for $\alpha = 60°$, 300 W, and 0.3 Pa. FRONT label indicates the area closest to the target, whilst BACK indicates the furthest part of the substrate from the target. b) Picture of samples deposited under non-restricted (left) and restricted (right) OAD conditions. The generated anisotropy across the sample is observed by the naked eye. c) Columnar tilting angle β and thickness variation across the restricted sample. Distance from the front is defined as the distance between the point where the sputtered atoms reach first in the substrate, in other words, the closest point of the sample to the target. Samples are 20×20 mm² squares, as said previously, therefore the distance from the front 20 mm corresponds to the furthest part of the sample from the target (i.e., "back"). The theoretical value calculated by means of the cosine rule (Equation 3) is depicted with a red line to show how the anisotropy can generate angles above the theoretical limit.

is punctual instead of distributed (Magnetron Sputtering), resulting in higher β values for the same materials (Table 1). However, with the use of a restricting mask configuration technology,[51] comparable and even higher β values have been reached. As a record value, it can be seen in Figure 7c the columnar inclination of 47.3°, an inclination never seen in a metal oxide thin film deposited by magnetron sputtering, to the best of our knowledge. In Figure 7c, it can also be seen how β values are close to the theoretical limit (calculated by the cosine rule (Equation 3)), even overlapping when the "back" of the sample is compared.

The anisotropy found in this work, generated by the working principle of the OAD and the use of a restrictor box, has the potential to produce diverse β angles on the same sample that could be exploited for such different applications (e.g., gas sensors, supercapacitors, acoustic sensors).[1–3] Also, if the interest is on β homogeneity, the area with the angles of interest could be diced and used for the desired purpose. The size of the uniform areas will be studied next by expanding the performed SEM analysis.

The new limits achieved by the application of the techniques and optimizations discussed in this section open the door to push even further the applicability of inclined films in advanced devices. Increasing the inclination of the films above the known levels will provide higher surface area for example for

sensing applications, improving the sensitivity of the device.[60] In optoelectronics applications, it has been demonstrated how the optical properties of materials can be tuned by means of OAD, also including the use of this technique for metamaterial fabrication.[61] As an example, with the current OAD procedures, scientists achieved the lowest refractive index material to the date, being $n \sim 1.05$ for SiO_2.[62] In that investigation, the material deposited by electron-beam evaporation, achieved a columnar inclination of $\beta = 45°$. With the implementation of the optimized process presented in this work, it would be possible to incline even further the structure and replace the costly evaporator by a more scalable magnetron sputtering technology, reaching lower refractive indexes for better anti-reflective coatings.

3.4. Deposition Time Effect of Inclined ZnO Films

The following study is performed under restricted conditions and all the measurements were performed in the center of the sample to ensure comparability between samples. **Figure 8a** shows the difference in the columnar β angle for ZnO deposited at room temperature (RT) and T_{ch} of 100 °C for short period of time (i.e., 30 min). It is observed how the columnar structure and the
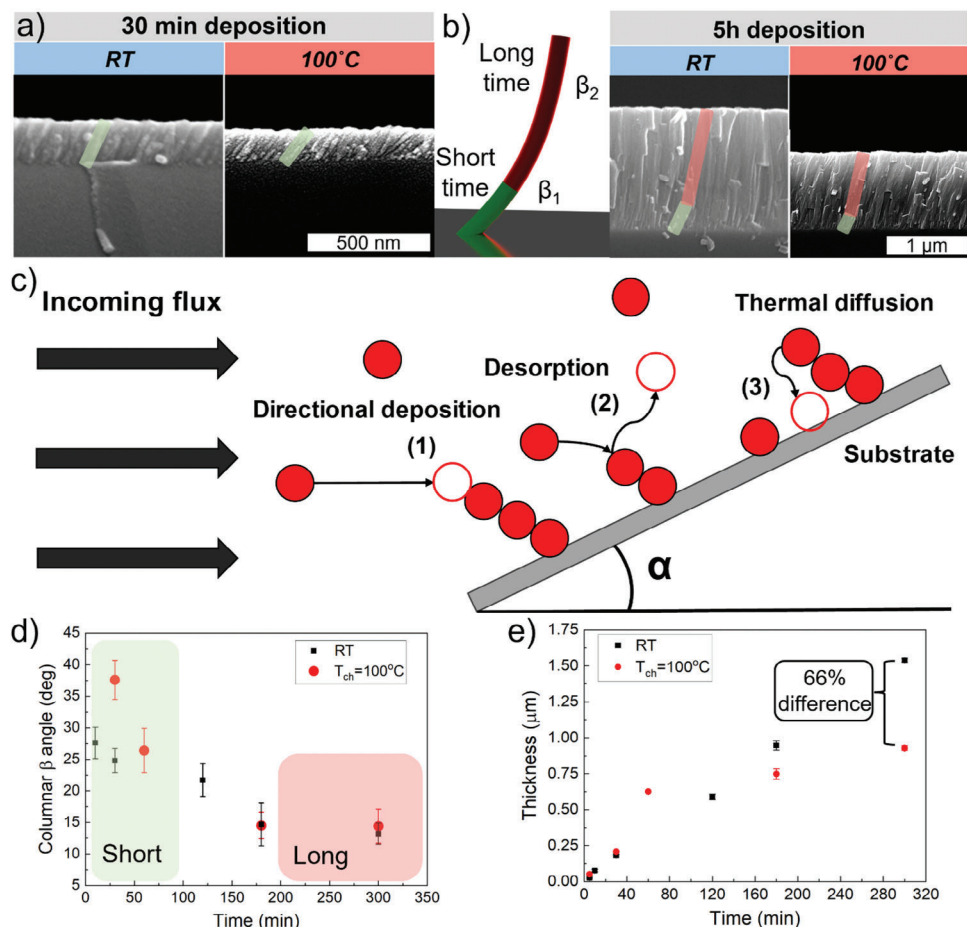
**ADVANCED
SCIENCE NEWS**

www.advancedsciencenews.com

**ADVANCED
PHYSICS
RESEARCH**

www.advphysicsres.com

Figure 8. a) SEM analysis for 30 min deposition at RT and T_{ch} of 100°C. Shadowed in green represents the inclination of the nanocolumns for short-time depositions. b) (Left) Schematic showing the bending of the structure when depositing for long-time depositions marked in red, and the original straight column at short deposition stages marked in green. (Right) SEM analysis for 5 h deposition at RT and T_{ch} of 100 °C. Shadowed in green and red represent the first and the latter stages of the deposition following the gradual decrease of columnar angle across the thickness. c) Diagram representing the three potential scenarios of an OAD process. 1) Corresponds to the natural OAD atom that is deposited with high directionality and low adatom diffusion. It contributes with efficiency to the overall shadowing mechanism that leads to highly inclined films.[34] 2) Comprises any desorption process happening naturally in any sputtering process, the atom that reaches the substrate does not stick to the surface and it is expulsed back to the environment. 3) Represents the thermal diffusion mechanism where atoms that reach the surface of the substrate and are deposited at the top of an existing nanocolumn diffuse in the films due to the increased thermal energy available in the system (i.e., temperature), relocating in vacated areas in the film. d) Columnar angle β as a function of the deposition time for depositions applying 100 °C and no intentional heating during the growth. The results indicate a decrease in the resulting angle for both datasets when depositing for longer times. Shadowed areas represent the stages described previously for short and long depositions. e) Thickness evolution as a function of the deposition time for depositions applying 100 °C and no intentional heating during the growth. There exists a thermal diffusion effect when depositing for long times (t_{dep}>5 h) and temperature. This effect causes the film thickness to decrease by 66% compared to the non-heated deposition, due to the increased atomic diffusion caused by the heating during the deposition.

thickness remain similar, however, there exists a slight difference in the inclination due to the effect of the temperature. This effect could be explained by the intrinsic increase of the MFP (Equation 2) when the atoms in the discharge plasma have extra energy available (i.e., thermal energy). For the same deposition conditions (working pressure of 0.3 Pa), the MFP increases from 42 to 53 mm by increasing the chamber temperature to 100°C. Therefore, bringing the system closer to ideal ballistic conditions (MFP > 70 mm (target-to-sample distance)) which would enhance the directionality of the deposition, allowing the increase of the resulting columnar β angle of ZnO thin films. In Figure 8a an increase of ≈50% in the columnar angle β is observed for the 100 °C

deposited sample, compared to the RT sample. Figure 8b, however, shows that for long deposition times (t_{dep}>5 h) the structure inclination gradually loses the initial angle (β_1), observed during the first stages of the growth, and bends toward lower angles (β_2) as the deposition continues. This behavior is observed for both samples deposited at RM and 100 °C (Figure 8b). This observation would indicate in the long term, thermal diffusion effects are dominating over the influence of the shadowing mechanism on the resulting film. At RT conditions, thermal diffusion mechanisms occur at long deposition times due to the unintentional gradual increase in the chamber temperature happening when the plasma is maintained in time. For 100 °C, the effect is more

**ADVANCED
SCIENCE NEWS**

www.advancedsciencenews.com

**ADVANCED
PHYSICS
RESEARCH**
Open Access

www.advphysicsres.com

prominent due to the constant application of temperature since the commencement of the deposition process. Additionally, in terms of the film thickness, it is observed in Figure 8b a significant reduction when comparing long deposited samples with and without the application of temperature. The difference in thickness starts being significant for deposition times over 5 h where the deposition rate decreases from 0.31 to 0.19 μm h^{-1}. This reduction, can be attributed to a certain atomic diffusion happening naturally when allowing the atoms to slightly diffuse and reorganize forming a more compact layer, filling the naturally occurring porous structure generated during an OAD process. Figure 8c, displays a diagram of the mechanisms involved in the OAD process to further understand this competition of effects. To simplify the process, we could divide into three the potential scenarios the atoms can exhibit when reaching the substrate surface. Depicted with (1), it represents the directional deposition of the atoms coming in a straight line from the target. That is directly contributing to the shadowing effect, as it allows the columns to grow in the desired inclination. In Figure 8c, it can also be observed the desorption mechanism (2), happening naturally in any PVD process, where the atom that reaches the surface of the substrate does not contribute to the film growth and is desorbed back to the environment. Finally, (3) is the mechanism that represents thermal diffusion, and it is only activated when an increase in the chamber temperature occurs. This mechanism directly competes with (1), as it would allow the atoms to reposition themselves in the structure, losing the direction achieved by the shadowing effect. Therefore, reducing the overall inclination of the film. For the best OAD process, it would then be necessary to enhance mechanism (1) and reduce mechanism (3). In other words, improving the directionality of the deposition (e.g., decreasing the work pressure or restricting the flux, as seen in Section 3.2 and 3.3, respectively), and keeping the temperature low.

Figure 8d,e represent the evolution of the columnar inclination angle β and the thickness of the ZnO thin film, respectively, with the deposition time, studied at T_{ch} of RT (black squares in the figure) and at 100 °C (red circles in the figure). A decreasing trend could be observed from the results, indicating the shadowing effect (Figure 8c-1) dominates the first stage of the deposition allowing the atoms to reach the substrate in a more directional deposition, therefore reaching higher β values. However, for longer depositions where the substrate reaches higher temperatures, there exists a competition between shadowing and thermal diffusion mechanisms[34] (Figure 8c-1–3).

To further expand this study in the future, we propose repeating the deposition set with "cooling down" stages for long-time depositions to investigate the evolution of the inclined structure when the shadowing mechanism predominates over thermal effects continuously during the growth process. That could be achieved with a cooled substrate holder or including intervals where the plasma is turned off, both to reduce the thermal diffusion mechanisms. Additionally, to enhance the directionality of the deposition, hence the shadowing mechanism, the set of depositions will be combined with the restrictor technology utilized in Section 3.3. As other works reported, the effect of the substrate temperature on the resulting columnar inclination is still under investigation, and more research needs to be done in the field to understand the mechanisms behind the observed effects.[63]

Some works reported in the literature present opposite results, with cases where β is lower for higher substrate temperatures [40,64,65] and others that β is higher when increasing the substrate temperature.[41,66,67]

4. Conclusion

In this paper, we demonstrated an efficient and simple method to produce ultra-inclined nanocolumnar thin films by implementing a novel restricted OAD method in a conventional MS. One of the biggest drawbacks for the utilization of MS being the large, distributed source of atoms, has here been compensated by the use of the restricting technology,[51] allowing to reach $\beta \approx 47°$ (close to theoretical values (Equation 3)). It has thoroughly been investigated how OAD of ZnO thin film nanostructure using DC reactive magnetron sputtering could be tuned by means of varying different deposition parameters to obtain highly inclined nanostructured metal oxide thin films. The paper also shows, with the optimization of the magnetron power (300 W), as seen for metals, how reducing the pressure during deposition leads to an increase in the resulting β angles for ZnO thin films. Improving the ballistic conditions of the deposition limits the interatomic scattering processes allowing more directional depositions, which is key for OAD. Second, it has been confirmed the improvement in the directionality of the deposition when using the patented technology from this work, by Novosound Ltd, allows restricting the incoming sputtered flux of atoms with a fabricated restrictor box that only allows the atoms coming in a straight line from the large Zn target to reach the substrate surface. This slit collimation allowed not only the obtention of higher columnar tilting angles β but also the improvement of the reproducibility of the DC-RMS OAD process across multiple depositions which is key for this technique to be exploited in industrial applications. Moreover, it has been found by finite element analysis simulations and empirical studies that restricting the flux generates a β angle distribution across the sample, allowing the growth of multizonal angular areas in a single deposition. Finally, it has been demonstrated how the columnar tilting angle β is affected when depositing for longer times whilst keeping the other deposition parameters steady but the temperature. This study resulted in the discovery of two stages for the deposition with time, short and long times (t_{dep}>5 h). Additionally, it was demonstrated the increase of MFP when increasing the T_{ch} allowing the further increase of β, significant for short depositions (t_{dep}<5 h). For long deposition times, a reduction in the film thickness is observed when applying temperature, mainly due to the excess of energy allowing the surface diffusion of atoms, compacting the film, allowing the structure to reorganize and achieve a denser packed film.

Enhancing the tilting angle of ZnO films close to the theoretical values enables us to present the restricted MS-OAD as an appreciated method to produce the best version of inclined ZnO for a number of sensing applications requiring an ultra-inclined nanostructured film. Further studies would include the engineering of an ultrasonic nanostructured thin film transducer by the use of the knowledge acquired during the investigation in this work to finely achieve the desired material properties and enhance the sensing capabilities.

Supporting Information

Supporting Information is available from the Wiley Online Library or from the author.

Acknowledgements

Conflict of Interest

The authors declare no conflict of interest.

Author Contributions

MPG and CGN conceptualized the work; MPG carried out the synthesis and characterization of ZnO films with support from KM, DG, DH and CGN; DH and CGN funded the project; MPG and CGN wrote the manuscript with support from all co-authors; CGN and DH provided overall supervision for the project; All authors have approved the final version of the manuscript.

Data Availability Statement

The data that support the findings of this study are available from the corresponding author upon reasonable request.

Keywords

[1] R. Hanson, L. P. Kouwenhoven, J. R. Petta, S. Tarucha, L. M. K. Vandersypen *Rev. Mod. Phys.* **2007**, *79*, 1217.

[2] R. Weigel, D. P. Morgan, J. M. Owens, A. Ballato, K. M. Lakin, K. Hashimoto, C. C. W. Ruppel, *I E E E Trans Microw Theory Tech* **2002**, *50*, 738.

[3] C. Campbell *Surface Acoustic Wave Devices and their Signal Processing Applications*. Elsevier, Amsterdam **1989**.

[4] Y.-Q. Fu, H.-F. Pang, H. Torun, R. Tao, G. McHale, J. Reboud, K. Tao, J. Zhou, J. Luo, D. Gibson, J. Luo, P. A. Hu *Lab Chip* **2021**, *21*, 254.

[5] K. D. Harris, A. Huizinga, M. J. Brett *Electrochem. Solid-State Lett.* **2002**, *5*, H27.

[6] J. J. Steele, J. P. Gospodyn, J. C. Sit, M. J. Brett *IEEE Sens. J.* **2006**, *6*, 24.

[7] W. Sucharitakul, A. Sukee, P. Leuasoongnoen, M. Horprathum, T. Lertvanithphol, P. Janphuang, P. Mitsomwang, B. Sindhupakorn *Mater. Res. Express* **2021**, *8*, 125702.

[8] M. M. Hawkeye, M. J. Brett *J. Vac. Sci. Technol., A* **2007**, *25*, 1317.

[9] W. Zhou, J. Brock, M. Khan, K. F. Eid *J. Magn. Magn. Mater.* **2018**, *456*, 353.

[10] A. S. Dev, A. K. Bera, P. Gupta, V. Srihari, P. Pandit, M. Betker, M. Schwartzkopf, S. V. Roth, D. Kumar *Appl. Surf. Sci.* **2022**, *590*, 153056.

[11] J. K. Jochum, T. Saerbeck, V. Lazenka, V. Joly, L. Shan, H.-G. Boyen, K. Temst, A. Vantomme, M. J. Van Bael *J. Magn. Magn. Mater.* **2019**, *483*, 76.

[12] A. K. Bera, A. S. Dev, M. Kuila, M. Ranjan, P. Pandit, M. Schwartzkopf, S. V. Roth, V. R. Reddy, D. Kumar *Appl. Surf. Sci.* **2022**, *581*, 152377.

[13] X. Xiao, G. Dong, J. Shao, H. He, Z. Fan *Appl. Surf. Sci.* **2010**, *256*, 1636.

[14] Y. He, J. Fu, Y. Zhao *Front Phys.* **2014**, *9*, 47.

[15] T. Motohiro, Y. Taga *Appl. Opt.* **1989**, *28*, 2466.

[16] M. M. Hawkeye, M. T. Taschuk, M. J. Brett *Glancing Angle Deposition of Thin Films* Wiley, New York **2014**.

[17] M. T. Taschuk, M. M. Hawkeye, M. J. Brett *in Handbook of Deposition Technologies for Films and Coatings*, William Andrew Publishing, Norwich, NY **2010**, p. 621–678.

[18] A. Lakhtakia, R. Messier *Sculptured Thin Films: Nanoengineered Morphology and Optics*. vol. *59*. SPIE, France **2005**. https://doi.org/10.1117/3.585322.

[19] M. Link, J. Weber, M. Schreiter, W. Wersing, O. Elmazria, P. Alnot *Sens Actuators B Chem* **2007**, *121*, 372.

[20] Y. Q. Fu, J. K. Luo, X. Y. Du, A. J. Flewitt, Y. Li, G. H. Markx, A. J. Walton, W. I. Milne *Sens Actuators B Chem* **2010**, *143*, 606.

[21] X. He, H. Guo, J. Chen, W. Wang, W. Xuan, Y. Xu, J. Luo *Appl. Phys. Lett.* **2014**, *104*, 1.

[22] S. Bensmaine, L. Le Brizoual, O. Elmazria, J. J. Fundenberger, M. Belmahi, B. Benyoucef *Diam Relat Mater* **2008**, *17*, 1420.

[23] T. Yanagitani, N. Morisato, S. Takayanagi, M. Matsukawa, Y. Watanabe *IEEE Trans Ultrason Ferroelectr Freq Control* **2011**, *58*, 1062.

[24] H.-F. Pang, R. Tao, J. Luo, X. Zhou, J. Zhou, G. McHale, J. Reboud, H. Torun, D. Gibson, K. Tao, H. l. Chang, Y.-Q. Fu *Surf. Coat. Technol.* **2022**, *442*, 128336.

[25] D. Fakult, G. Doctor, C. Gr, S. Gutachter, B. R. Prof Oblique Angle Deposition of Thin Films – Theory, Modelling, and Application, PhD Thesis, Universität Leipzig, **2019**.

[26] A. Barranco, A. Borras, A. R. Gonzalez-Elipe, A. Palmero *Prog. Mater. Sci.* **2016**, *76*, 59.

[27] P. J. Kelly, R. D. Arnell *Vacuum* **2000**, *56*, 159.

[28] X. S. Zhou, C. Zhao, R. Hou, J. Zhang, K. J. Kirk, D. Hutson, Y. J. Guo, P. A. Hu, S. M. Peng, X. T. Zu, Y. Q. Fu *Ultrasonics* **2014**, *54*, 1991.

[29] K. J. Kirk, J. Elgoyhen, J. P. Hood, D. Hutson *J. Electroceram.* **2011**, *27*, 29.

[30] J. M. García-Martín, R. Alvarez, P. Romero-Gómez, A. Cebollada, A. Palmero *Appl. Phys. Lett.* **2010**, *97*, 1.

[31] R. Álvarez, L. González-García, P. Romero-Gómez, V. Rico, J. Cotrino, A. R. Gonzlez-Elipe, A. Palmero *J Phys D Appl Phys* **2011**, *44*, 385302.

[32] A. Garcia-Valenzuela, S. Muñoz-Piña, G. Alcala, R. Alvarez, B. Lacroix, A. J. Santos, J. C. Maraver, V. Rico, R. Gago, L. Vazquez, J. Cotrino, A. R. Gonzalez-Elipe, A. Palmero *Plasma Processes Polym.* **2019**, *16*, 1800153.

[33] S. Wang, G. Xia, H. He, K. Yi, J. Shao, Z. Fan *J. Alloys Compd.* **2007**, *431*, 287.

[34] R. Alvarez, C. Lopez-Santos, J. Parra-Barranco, V. Rico, A. Barranco, J. Cotrino, A. R. Gonzalez-Elipe, A. Palmero *J. Vac. Sci. Technol.* **2014**, *32*, 041802.

[35] H. F. Pang, Y. Q. Fu, R. Hou, K. J. Kirk, D. Hutson, X. T. Zu, F. Placido *Ultrasonics* **2013**, *53*, 1264.

[36] S. Bensmaine, L. Le Brizoual, O. Elmazria, J. J. Fundenberger, B. Benyoucef *Phys Status Solidi A Appl Mater Sci* **2007**, *204*, 3091

[37] H. F. Pang, G. A. Zhang, Y. L. Tang, Y. Q. Fu, L. P. Wang, X. T. Zu, F. Placido *Appl. Surf. Sci.* **2012**, *259*, 747.

[38] B. Bouaouina, C. Mastail, A. Besnard, R. Mareus, F. Nita, A. Michel, G. Abadias *Mater. Des.* **2018**, *160*, 338.

[39] L. C. Chen, C. H. Tien, W. C. Liao, Y. M. Luo *J. Lumin.* **2011**, *131*, 1234.

[40] J. Dervaux, P.-A. Cormier, P. Moskovkin, O. Douheret, S. Konstantinidis, R. Lazzaroni, S. Lucas, R. Snyders *Thin Solid Films* **2017**, *636*, 644.

**ADVANCED
SCIENCE NEWS**

www.advancedsciencenews.com

**ADVANCED
PHYSICS
RESEARCH**
Open Access

www.advphysicsres.com

[41] S. Liedtke, C. Grüner, J. W. Gerlach, B. Rauschenbach *Beilstein J. Nanotechnol.* **2018**, *9*, 954.

[42] W. Phae-ngam, M. Horprathum, C. Chananonnawathorn, T. Lertvanithphol, B. Samransuksamer, P. Songsiriritthigul, H. Nakajima, S. Chaiyakun *Curr. Appl. Phys.* **2019**, *19*, 894.

[43] C. Jetjamnong, S. Chotikaprakhan, R. Kowong, C. Chananonnawathorn, A. Bootchanont, T. Lertvanithphol, S. Limwichean, P. Kijamnajsuk, A. Klamchuen, G. Meng, A. Watcharapasorn, H. Nakajima, M. Horprathum *Vacuum* **2022**, *196*, 110777.

[44] J. M. Niewehuizen, H. B. Haanstra *Philips Tech. Rev.* **1966**, *27*, 87.

[45] R. Alvarez, C. Lopez-Santos, J. Parra-Barranco, V. Rico, A. Barranco, J. Cotrino, A. R. Gonzalez-Elipe, A. Palmero *J. Vac. Sci. Technol. B* **2014**, *32*, 041802.

[46] A. Siad, A. Besnard, C. Nouveau, P. Jacquet *Vacuum* **2016**, *131*, 305.

[47] D. Deniz, R. J. Lad *J. Vac. Sci. Technol., A* **2011**, *29*, 011020.

[48] C. Patzig, B. Rauschenbach *J. Vac. Sci. Technol., A* **2008**, *26*, 881.

[49] S. Flickyngerová, M. Netrvalová, P. Šutta, I. Novotný, V. Tvarožek, P. Gašpierik, J. Bruncko *Thin Solid Films* **2011**, *520*, 1233.

[50] M. Link, M. Schreiter, J. Weber, R. Gabl, D. Pitzer, R. Primig, W. Wersing, M. B. Assouar, O. Elmazria *J. Vac. Sci. Technol., A* **2006**, *24*, 218.

[51] M. Pelayo Garcia, C. Garcia Nuñez, D. Gibson, D. Hughes, *GB2313815.9*, **2023**.

[52] C. Thring, F. Band, D. Irving, K. McAughey, D. Hughes, In *2020 IEEE International Ultrasonics Symposium (IUS)*, IEEE, 2020; Vol. 2020-Septe, pp 1–3.

[53] Q. Zhou, S. Lau, D. Wu, K. Kirk Shung *Prog. Mater. Sci.* **2011**, *56*, 139.

[54] C. T. Rueden, J. Schindelin, M. C. Hiner, B. E. DeZonia, A. E. Walter, E. T. Arena, K. W. Eliceiri *BMC Bioinformatics* **2017**, *18*, 529.

[55] COMSOL Multiphysics v. 6.2. www.comsol.com. COMSOL AB, Stockholm, Sweden.

[56] M. Pelayo Garcia, K. L. McAughey, D. Gibson, D. A. Hughes, C. Garcia Nunez, presented at *13th Spanish Conf. on Electron Devices (CDE)*, Seville, June, **2021**. https://doi.org/10.1109/CDE52135.2021. 9455746.

[57] E. Chason, P. R. Guduru *J. Appl. Phys.* **2016**, *119*, 191101.

[58] U. Holzwarth, N. Gibson *Nat. Nanotechnol.* **2011**, *6*, 534.

[59] R. N. Tait, T. Smy, M. J. Brett *Thin Solid Films* **1993**, *226*, 196.

[60] K. M. Byun, N.-H. Kim, J. W. Leem, J. S. Yu *Appl. Phys. B* **2012**, *107*, 803.

[61] J. G. Gibbs, A. G. Mark, S. Eslami, P. Fischer *Appl. Phys. Lett.* **2013**, *103*, 213101.

[62] J.-Q. Xi, M. F. Schubert, J. K. Kim, E. F. Schubert, M. Chen, S.-Y. Lin, W. Liu, J. A. Smart *Nat. Photonics* **2007**, *1*, 176.

[63] R. Mareus, C. Mastail, F. Nita, A. Michel, G. Abadias *Comput. Mater. Sci.* **2021**, *197*, 110662.

[64] A. Panepinto, R. Snyders *Nanomaterials* **2020**, *10*, 2039.

[65] T. Hashimoto, K. Okamoto, K. Hara, M. Kamiya, H. Fujiwara *Thin Solid Films* **1982**, *91*, 145.

[66] L. Abelmann, C. Lodder *Thin Solid Films* **1997**, *305*, 1.

[67] V. Elofsson, D. Magnfält, M. Samuelsson, K. Sarakinos *J. Appl. Phys.* **2013**, *113*, 174906.